JACS
JOURNAL OF THE AMERICAN CHEMICAL SOCIETY
pubs.acs.org/JACS
Article

Monovalent Nickel-Mediated Radical Formation: A Concerted Halogen-Atom Dissociation Pathway Determined by Electroanalytical Studies

Qiao Lin, Yue Fu, Peng Liu,* and Tianning Diao*

Cite This: https://doi.org/10.1021/jacs.1c05255
Read Online

ACCESS | Metrics & More | Article Recommendations | Supporting Information

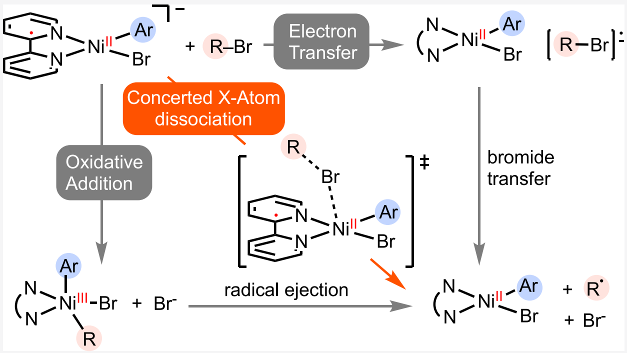

ABSTRACT: The recent success of nickel catalysts in stereoconvergent cross-coupling and cross-electrophile coupling reactions partly stems from the ability of monovalent nickel species to activate $C(sp^3)$ electrophiles and generate radical intermediates. This electroanalytical study of the commonly applied (bpy)Ni catalyst elucidates the mechanism of this critical step. Data rule out outer-sphere electron transfer and two-electron oxidative addition pathways. The linear free energy relationship between rates and the bond-dissociation free energies, the electronic and steric effects of the nickel complexes and the electrophiles, and DFT calculations support a variant of the halogen-atom abstraction pathway, the inner-sphere electron transfer concerted with halogen-atom dissociation. This mechanism accounts for the observed reactivity of different electrophiles in cross-coupling reactions and provides a mechanistic rationale for the chemoselectivity obtained in cross-electrophile coupling over homocoupling.

■ INTRODUCTION

Nickel catalysts excel in conducting cross-coupling reactions of $C(sp^3)$ electrophiles, owing to the slow β-H elimination of Ni–alkyl intermediates.[1−4] The activation of $C(sp^3)$ electrophiles invokes alkyl radical formation arising from the interaction of monovalent nickel species with $C(sp^3)$ electrophiles (Scheme 1A).[5−13] This fundamental step has two significant consequences: (1) formation of the radical intermediate erases the initial stereochemistry in the substrate and thus creates opportunities for stereoconvergent coupling of racemic alkyl halides,[14,15] and (2) in cross-electrophile coupling reactions, $C(sp^2)$ and $C(sp^3)$ electrophiles are separately activated by different nickel species via different mechanisms, which accounts for the selectivity of cross-electrophile coupling over homocoupling.[13]

Stepwise and concerted pathways have been considered to account for Ni(I)-mediated radical formation from $C(sp^3)$ electrophiles: S_N2 oxidative addition followed by radical ejection,[16] electron transfer preceding homolytic cleavage of the carbon–halogen bonds,[17−22] and halogen-atom abstraction (Scheme 1B).[10,23−25] DFT calculations support the halogen-atom abstraction mechanism in several nickel complexes.[10,23−25] Experimental efforts seeking to distinguish among these pathways have focused on well-defined (NHC)-Ni(I)[26] (NHC = *N*-heterocyclic carbene) and (xantphos)Ni(I) complexes.[27] Kinetic studies suggest that (xantphos)Ni(I)-mediated radical formation proceeds through halogen-atom abstraction. Such studies, however, have not been carried out with the most reactive catalytic systems, such as with bipyridines (bpy), since the isolation of such active Ni(I)–aryl complexes is challenged by their instability.[28]

The dilemma between the desire to study catalytically active species and their instability that hampers isolation has historically been solved by electroanalytical methods, allowing for kinetic measurements of *in situ* generated transient organometallic intermediates.[29−32] Recent cyclic voltammetry (CV) studies have shed light on the activation of benzyl bromides by Co(I) complexes.[33,34] With respect to Ni(I)-mediated radical formation from $C(sp^3)$ electrophiles, previous electroanalytical studies have focused on macrocyclic[17−22] and five-coordinated Ni(I) complexes,[35] which are not directly relevant to cross-coupling reactions. The latter example demonstrates that different ligands can alter the pathways.[35] Despite previous electrochemical studies of catalytic reactions[36−39] and the electronic structure of low-valent nickel species,[40,41] the mechanism of (bpy)Ni(I)-mediated activation of $C(sp^3)$ electrophiles has not been elucidated. The

Received: May 22, 2021

Scheme 1. Nickel(I)-Mediated Radical Formation as an Intermediate Step in Cross-Coupling Reactions (A) and Possible Pathways (B)

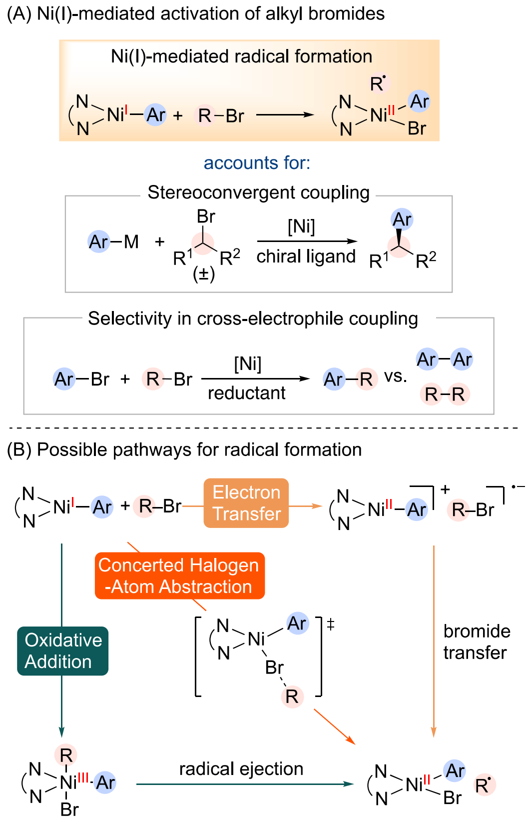

mechanistic significance of (bpy)Ni-mediated radical formation as an intermediate step in cross-coupling reactions, in combination with the growing participation of nickel complexes in electrocatalysis,[42−44] prompted us to carry out a comprehensive CV study to uncover the mechanism of alkyl halide activation by a (bpy)Ni(I) species (bpy = bipyridine). Our data compare the reactivity of different electrophiles and account for the observed selectivity in catalytic cross-electrophile coupling reactions.

■ RESULTS

Comparing the Activation Rates of Different Electrophiles. We conducted CV studies on (bpy)Ni(Mes)Br **1** as a model complex (Figure 1).[45] At −60 °C, the solution of **1** displays an electrochemically reversible CV wave (Figure 1A, blue trace). We assign the cathodic peak to the one-electron reduction of **1** to afford $[(bpy)Ni(Mes)Br]^{•-}$ (**2**, eq 1). The current peaks are proportional to the concentration of the species undergoing electron transfer and its diffusion coefficient according to the Randles−Sevcik equation, where i_p is the peak current, n is the number of electrons for the Ni redox couple, F is the Faraday constant, A is the surface area of the working electrode, C^0_{Ni} is the concentration of **1**, R is the ideal gas constant, T is the temperature, v is the scan rate, and D_{Ni} is the diffusion coefficient of **1** (eq 2).[46,47] The near 1:1 ratio of peak anodic current (i_{pa}) to cathodic current (i_{pc}), together with the lack of a dependence of i_{pa}/i_{pc} on the scan rate [Figure S1, Supporting Information (SI)], suggests that the initial **1** can be recovered after the forward and reverse scan cycles and that **2** is stable on the CV time scale.

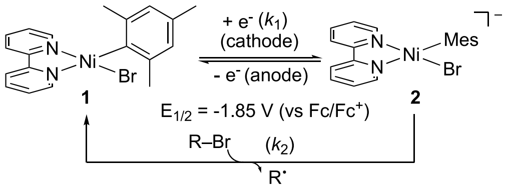

(1)

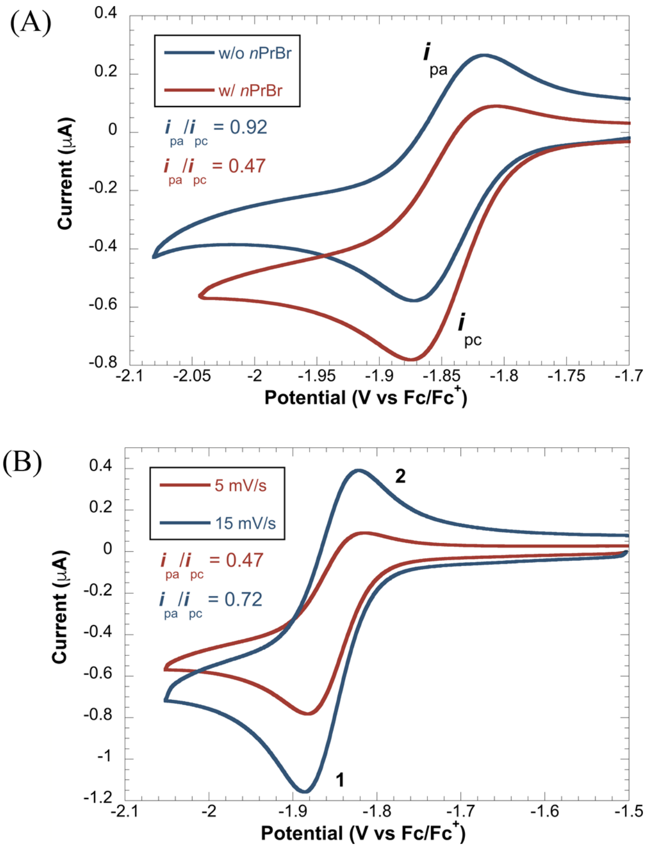

Figure 1. Variation of the peak current ratio (i_{pa}/i_{pc}) in the CV of (bpy)Ni(Mes)Br (**1**) in the presence and absence of 10 mM 1-bromopropane with a scan rate of 5 mV/s (A) and at different scan rates (B). CVs were run with 1.0 mM **1** in a 600 mM solution of Bu_4NBr in DMF at −60 °C, using a 0.071 cm^2 glassy carbon working electrode.

$$i_p = 0.4463nFAC^0_{Ni}\sqrt{\frac{nFvD_{Ni}}{RT}} \qquad (2)$$

In the presence of an electrophile, such as 1-bromopropane, the CV becomes quasireversible with a decreased ratio of i_{pa}/i_{pc} (Figure 1A, red trace). We attribute this observation to an electrochemical mechanism (EC): The reduction of **1** at the cathode is followed by the oxidation of **2** with 1-bromopropane that depletes **2** and thus decreases the anodic peak current (i_{pa}) (eq 1). The ratio of i_{pa}/i_{pc} thus varies as a function of the scan rate (v), corresponding to the time allowed for **2** to react with 1-bromopropane between the two peak current measurements (Figure 1B). Varying the scan rate enabled the measurements of a series of i_{pa}/i_{pc} ratios, corresponding to different degrees of consumption of **2** by 1-bromopropane. Correlating i_{pa}/i_{pc} to the concentration of **2** allowed us to draw the time course for the reaction of **2** with 1-bromopropane (Figure 2A). Fitting the time course to a second-order kinetic model gave a rate constant of 5.9×10^{-1} M^{-1} s^{-1}.

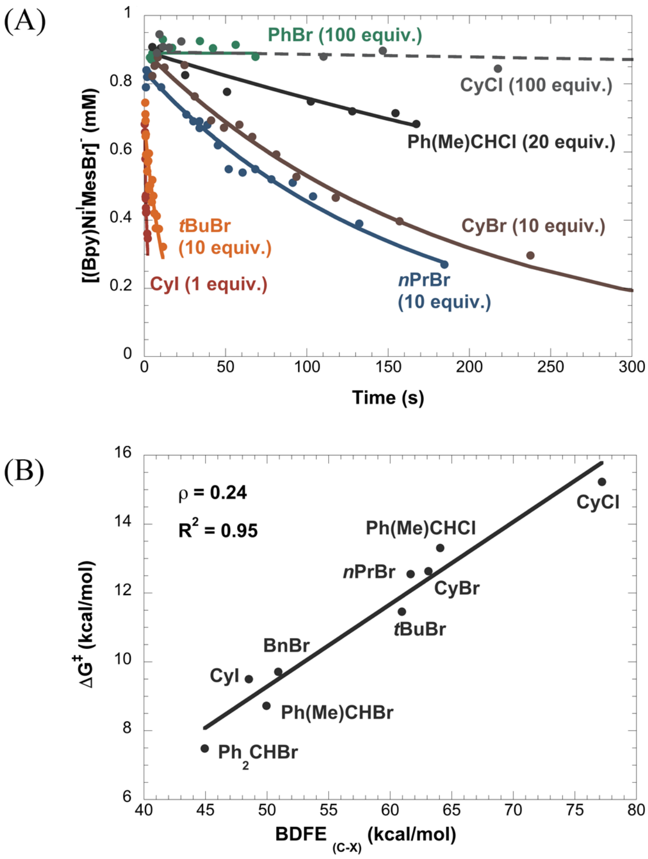

Figure 2. Time course of electrochemically generated $[(bpy)Ni(Mes)Br]^{\bullet -}$ (**2**) in the presence of different electrophiles (A) and the linear free-energy relationship between the activation energy ($\Delta G^{\ddagger}$) and the BDFE of carbon−halogen bonds (B). CVs were conducted with 1.0 mM (bpy)Ni(Mes)Br (**1**) in a 600 mM solution of Bu_4NBr in DMF at −60 °C. Data were generated by varying the scan rates from 5 to 1000 mV/s. The fittings of the time courses were simulated by COPASI.[49]

We applied this technique to investigate the reaction rates of **2** with a range of electrophiles (Figure 2A). With 100 equiv of PhBr, no conversion of **2** was observed over 70 s. Among C(sp^3) electrophiles, cyclohexyl chloride was inert, but modest reactivity was observed with 1-phenylethyl chloride. A variety of alkyl bromides proceeded to react with **2** at different rates. Cyclohexyl iodide reacted substantially faster than cyclohexyl bromide. Plotting the $\Delta G^{\ddagger}$ of these reactions as a function of the bond dissociation free energy (BDFE) of the carbon−halogen bonds gave a linear correlation with a slope of 0.24 (Figure 2B).[48]

Comparing the Rate of Bromide Dissociation to That of Electrophile Activation. Data collection at −60 °C was complicated by temperature fluctuations. We conducted subsequent CV studies at 22 °C. A new anodic peak appeared at a more positive potential, which is assigned to the oxidation of (bpy)Ni(I)(Mes) (**3**), raised from the dissociation of bromide from **2** (Figure 3, blue trace and the inset).[40] By varying the scan rate and measuring the corresponding shifts of the cathodic peak on the potential scale, we determined the first-order rate constant of bromide dissociation from **2** to be 2.5 s^{-1} at 22 °C (*cf.* Figure S3, SI).

In the presence of 100 equiv of BnBr at 22 °C, the CV of **1** became irreversible (Figure 3, green trace). The lack of an anodic current peak (i_{pa}) reflects rapid oxidation of electrochemically generated **2** by BnBr (k_2). The significantly higher cathodic current peak (i_{cat}) relative to i_{pc} indicates an electrocatalysis process (EC′), where Ni(I) **2** serves as a catalyst that mediates the electroreduction of BnBr (eq 3).[30,46]

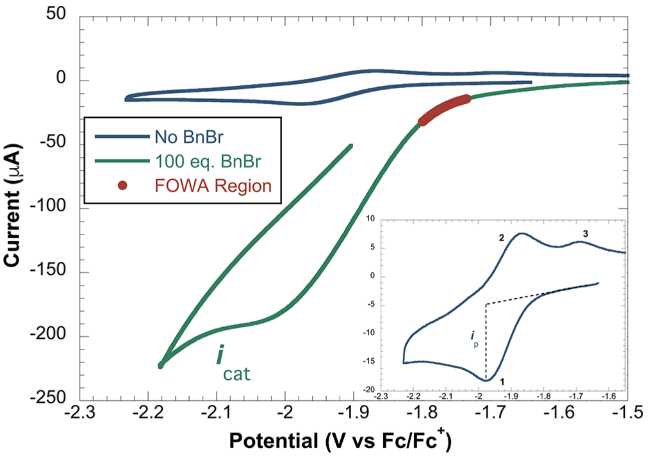

Figure 3. Cathodic sweeps of CVs of 1.0 mM (bpy)Ni(Mes)Br (**1**) in a 100 mM solution of Bu_4NBF_4 in DMF at 22 °C in the absence (blue trace and inset) and presence of 100 equiv BnBr (red trace). Scan rate = 500 mV/s.

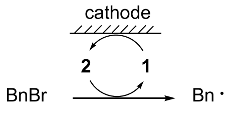

(3)

In this scenario, the current is created by the electrocatalytic turnover of **2** occurring at the electrode.[50] The increase of electrophile concentration accelerates the turnover rate of nickel and, thus, a higher cathodic current (i_{cat}) (Figure S4, SI). Increasing the BnBr loading to 100 equiv, however, was insufficient to reach the KS zone, in the sense that no plateau was observed.[29]

We adopted the "foot-of-the-wave" (FOW) analysis of the background-corrected CV to determine the reaction rate of **2** with BnBr (k_{obs}) under EC′ conditions.[51−53] At the foot-of-the-wave, i_{cat}/i_{pc} at a given potential (E) is described by a linear function of $\{1 + \exp[(F/RT)(E - E_{1/2(Ni^{II}/Ni^{I})})]\}^{-1}$ with the slope dependent on the scan rate (ν) and k_{obs} (eq 4). FOW analysis of the CV of **1** in the presence of 100 equiv BnBr (Figure 3, red trace) determined the pseudo-first-order rate constant, k_{obs}, to be 4.0 × 10^3 s^{-1} (Figure S5, SI), corresponding to a second-order rate constant k_4 of 4.0 × 10^4 M^{-1} s^{-1} (Scheme 2).

$$\frac{i_{cat}}{i_p} = \frac{2.24n\sqrt{\frac{RTk_{obs}}{F\nu}}}{1 + \exp\left[\frac{F}{RT}(E - E_{1/2})\right]} \tag{4}$$

The drastically slower rate of bromide dissociation from **2** ($k_3 = 2.5\ s^{-1}$) relative to that of the consumption of **2** by BnBr ($k_4 = 4.0 \times 10^4\ M^{-1}\ s^{-1}$) reveals that **2** is directly oxidized by BnBr without forming **3** through bromide dissociation (Scheme 2). To obtain further support of this assignment, we determined the rate of **2**-mediated BnBr oxidation in the presence of Bu_4NBr (tetra-*n*-butylammonium bromide). If bromide dissociation takes place prior to the reaction of **2** with BnBr, we would observe inhibition by Bu_4NBr. The comparable rates of reaction in the absence (k_4) and presence

Scheme 2. Comparison of the Bromide Dissociation Rate with Oxidation of 2 by BnBr

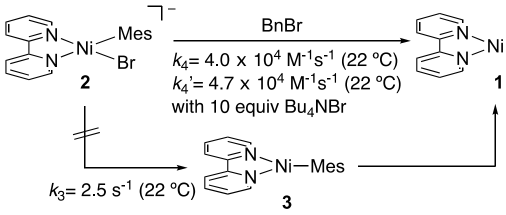

(k_4') of Bu_4NBr substantiate the lack of bromide dissociation under these conditions. This result is corroborated by the beneficial effect of halide salt additives, such as NaI or MgI_2, in cross-electrophile coupling reactions, suggesting that the presence of coordinating anions may serve to stabilize monovalent nickel intermediates.

Steric Effect of Ni(I)−Ar. FOW analysis equipped us with a convenient means to determine the electronic and steric effects of electrophiles and nickel species for the oxidation of Ni(I) by a C(sp^3) electrophile. Varying the aryl group on the Ni center reveals that steric hindrance decreases the reaction rate (Figure 4). In particular, the change of a 2,4-dimethylphenyl ligand to mesityl led to a drastic rate decrease.

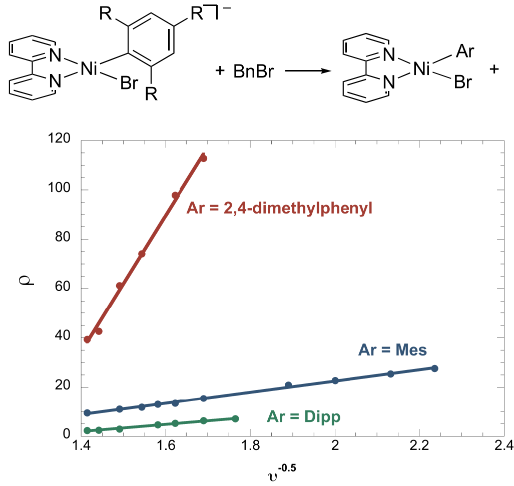

Figure 4. Steric effect of nickel complexes on activation of benzyl bromide: the slopes of FOW analysis plots against (scan rate)$^{-0.5}$. The slope of the linear fits is proportional to k_{obs}, according to eq 4. Reaction conditions: 1.0 mM (bpy)Ni(Ar)Br in a 100 mM solution of Bu_4NBF_4 in DMF at 22 °C, BnBr = 100 mM.

Electronic Effect of the Electrophile. A Hammett study of benzyl bromide derivatives with various *para/meta*-substituents sheds light on the electronic effect of the C(sp^3) electrophile. Both electron-rich and electron-deficient substituents accelerated the reaction (Figure 5A). We obtained excellent linear fittings for electron-rich and electron-deficient substrates with negative and positive slopes, respectively, by correlating them with σ^-. A break in the Hammett relationship may be assigned to a change in mechanism between stabilization of a positive and negative charge in the transition state or the formation of a radical intermediate at the benzylic position, which can be stabilized by either mesomerically donating or withdrawing groups.[54−56]

In order to delineate the electronic effect of electrophiles on oxidation of 2, we applied multiparameter linear regression analysis seeking to unify the Hammett model.[57] When correlating the rate data with Jiang's spin-delocalization substituent constants $\sigma^\bullet_{JJ}$, a parameter that describes the stabilization effect of a substituent to radicals,[58,59] we obtained fittings that underestimated the effect of electron-withdrawing substituents but overestimated that of electron-donating groups (Figure S6, SI). When utilizing both the charge factor (σ^-) and the radical factor ($\sigma^\bullet_{JJ}$) together to describe the electronic effect, we obtained a good linear correlation (Figure 5B). The positive coefficient for σ^- reveals the buildup of partial negative charges in the transition state. The radical term, $\sigma^\bullet_{JJ}$, with a larger coefficient, reflects a more significant stabilization of spin density in the transition state. Such a two-term linear free energy relationship is reminiscent of previous studies on reactions forming nucleophilic radical intermediates, such as halogen-atom abstraction.[33,54]

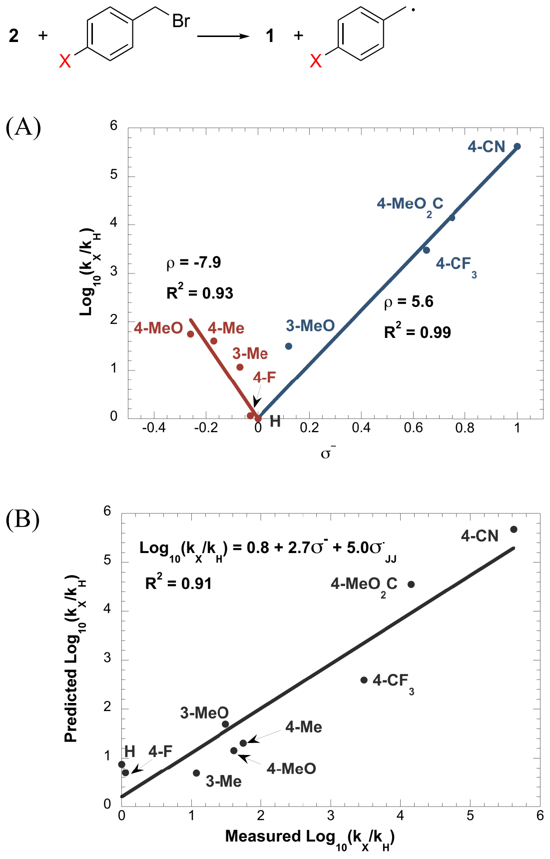

Figure 5. (A) Hammett plot for electrocatalytic oxidation of benzyl bromides catalyzed by **1**. Reaction conditions: 1.0 mM (bpy)Ni(Mes)Br (**1**) in a 100 mM solution of Bu_4NBF_4 in DMF at 22 °C, [$ArCH_2Br$] = 100 mM. k_x = k_{obs} of the electrocatalytic oxidation of benzyl bromides derived from FOW analysis. (B) Unified Hammett model, split into charge (σ^-) and radical ($\sigma^\bullet_{JJ}$) stabilization terms, for electrocatalytic oxidation of benzyl bromides catalyzed by **1**.

Electronic Effect of Ni(I)−Ar. We explored the electronic effect of the nickel complexes on the activation rate of benzyl bromide by varying the ligand and the *para*-substituents on the aryl group in (bpy)Ni(Ar)(Br) (Figure 6). The electronic effect of the substituents on the molecule is represented by their reduction potential $E_{1/2(Ni^{II}/Ni^{I})}$. The rate (k) of each reaction was determined by applying the FOW analysis as outlined above. While the use of 4,4′-di-*tert*-butylbipyridine resulted in a decrease of the reduction potential by 130 mV,

https://doi.org/10.1021/jacs.1c05255
J. Am. Chem. Soc. XXXX, XXX, XXX−XXX

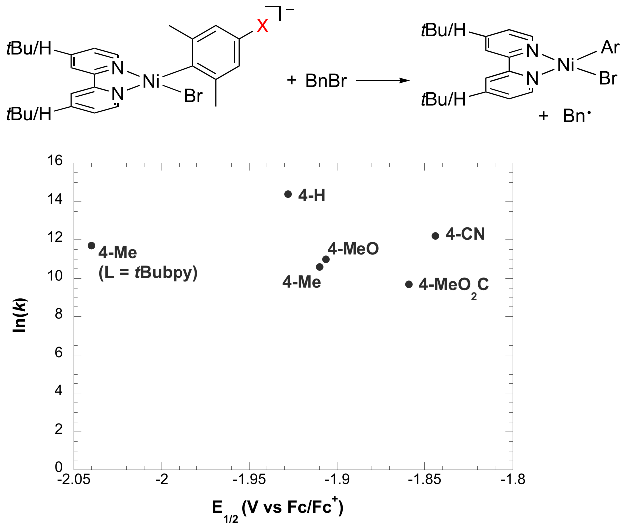

Figure 6. Electronic effect of Ni complexes. Rates (k_{obs}) are derived from FOW analysis. $E_{1/2}$ is the formal potential of the corresponding Ni(II)−aryl/Ni(I)−aryl couple, reflecting their electronic properties. Reaction conditions: 1.0 mM (bpy)Ni(Ar)Br **1** in a 100 mM solution of Bu_4NBF_4 in DMF at 22 °C, [BnBr] = 100 mM.

different *para*-substituents on the aryl ligand varied the redox potentials from −1.84 to −1.93 V. Despite the different reduction potentials, the reaction rates of these analogues to BnBr remain similar.

Electronic Structure of 2. The radical anion of (phen)-Ni(Mes)(Br) has been determined by EPR spectroscopy, featuring a redox-active phen ligand that stabilizes the Ni(II) center.[60] We performed a similar EPR analysis to elucidate the electronic structure of **2**. Reduction of **1** by 1 equiv of KC_8 led a color change from maroon to violet. EPR analysis of the solution at room temperature gave an isotropic signal with a *g* value of 2.0047 (Figure 7). Simulation of the spectrum assigns the hyperfine splitting to the coupling of the radical to nitrogen and hydrogen atoms on bpy. The observation of a bpy-centered radical suggests that **2** is best described as a Ni(II) stabilized by a bpy radical anion.[28] Moreover, EPR analysis of $[(4,4'\text{-di-}tert\text{-butylbipyridine})Ni(Mes)Br]^{\bullet-}$ gave a similar isotropic signal with a *g* value of 2.004 (Figure S8, SI), suggesting that the presence of electron-donating groups does not detract the redox activity.

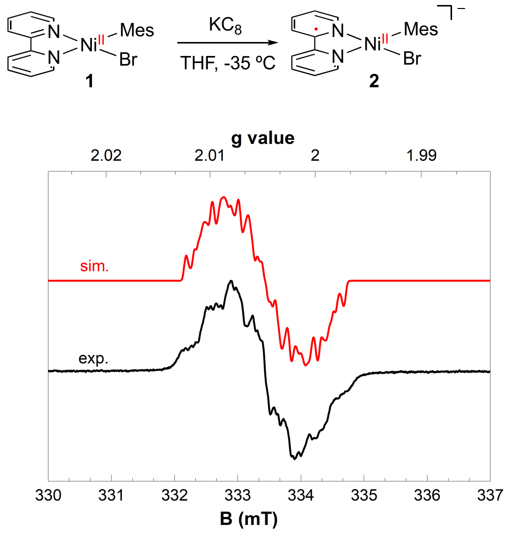

Figure 7. X-band EPR spectrum of **2** in THF. Temperature = 295 K, microwave frequency = 9.355 531 GHz, power = 0.6325 mW, modulation frequency = 1 mT/100 kHz, modulation amplitude = 0.5 G. The simulated spectrum (red) uses the following parameters: *g* = 2.0047, $A_{N,N,H,H,H}$ = [11.666, 8.3360, 7.2980, 5.8227, 3.7990] MHz.

Computational Studies. We performed density functional theory (DFT) calculations to explore the mechanism of $[(bpy)Ni(Mes)Br]^{\bullet-}$ (**2**)-mediated activation of BnBr. Because the computational results may be affected by the choice of the DFT method and basis set, we assessed different methods using the explicitly correlated local coupled-cluster method PNO-LCCSD(T)-F12[61] and the experimental activation free energies (Figure 5) as the reference. The details of the benchmark studies are provided in the Supporting Information. Several functionals, including BP86-D3, B3LYP-D3, and M06L, provide reasonable agreement with the experimental data. Although the use of BP86-D3 in single-point energy calculations led to a systematic underestimation of the activation free energy by several kilocalories/mole, the correlation with the experimental barriers with different electrophiles is comparable to the results obtained using B3LYP-D3. When comparing the relative activation energies of halogen-atom transfer and S_N2 pathways with the PNO-LCCSD(T)-F12 energy values, BP86-D3 provided the best agreement. Therefore, we chose the (U)BP86-D3/def2-TZVPP, SMD(DMF)//(U)B3LYP-D3/6-31G(d)-SDD level of theory in the computational study.

The ground state of **2** is computed to be a square planar doublet with a ligand-centered radical, consistent with the EPR data (Figure 7). A scan of the bromide dissociation reaction coordinate gave an activation energy ($\Delta E^{\ddagger}$) of 19.2 kcal/mol with respect to **2**, although no transition state could be located. The high barrier to bromide dissociation is consistent with the experimentally observed slower rate of this process compared to the reaction of **2** with BnBr (Scheme 2).

The evaluation of different pathways concludes with the inner-sphere electron transfer (ISET) concerted with halogen-atom dissociation (**TS1**) (Figure 8).[35,62,63] The early transition state, **TS1**, features a long Ni−Br distance of 3.82 Å, in which bpy remains redox-active. The NPA charge of −0.363 e^- reflects that substantial electron density developed at the benzylic carbon of BnBr. The C−Br−Ni bond angle in **TS1** is slightly bent (150.6°) due to the dispersion interaction between the Bn group and the bpy ligand. The computed activation free energy of $\Delta G^{\ddagger}_{DFT}$ = 7.4 kcal/mol is slightly lower than the experimental values determined in this study ($\Delta G^{\ddagger}_{exp}$ = 11.2 kcal/mol) and a prior report.[27] When the B3LYP-D3 or M06L functional was used in the single-point energy calculations in place of BP86-D3, a better agreement with $\Delta G^{\ddagger}_{exp}$ can be obtained (see Table S8, SI).

TS1 directly proceeds to form **1** and the benzyl radical upon the dissociation of the bromide anion, as evident from intrinsic reaction coordinate (IRC) calculations (Figure S40, SI). Although the Ni−Br distance slightly decreases after halogen-atom abstraction, a Ni−Br covalent bond is never fully formed along the reaction coordinate. After the cleavage of the Bn−Br bond, the Br^- spontaneously dissociates to form **1**. The steric hindrance of the mesityl ligand, the high stability of **1**, and the weak interaction between Br^- and Ni (Figure S41, SI) prevented the formation of a five-coordinated $[(bpy)Ni(Mes)Br_2]^-$ intermediate.

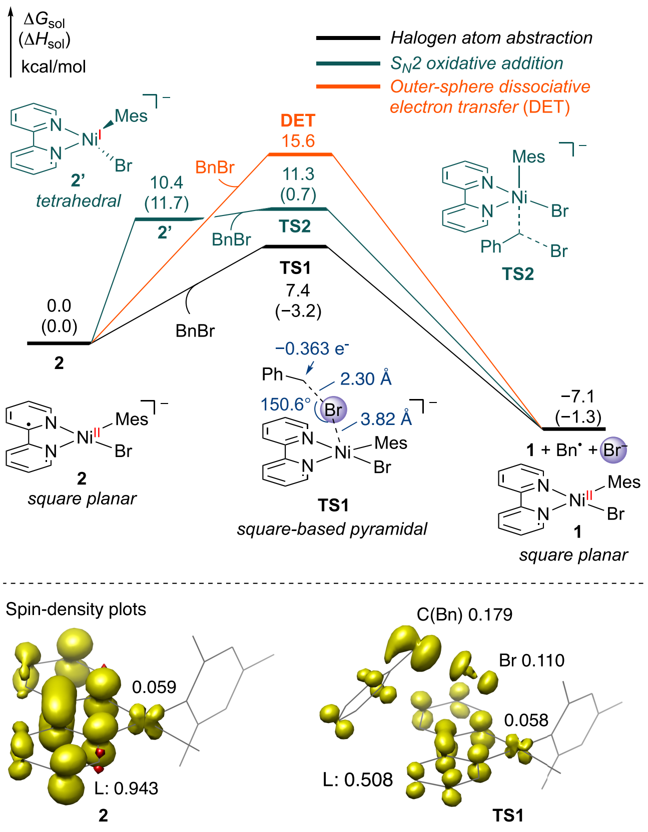

Figure 8. Computed reaction profiles of the oxidation of **2** by benzyl bromide.

The S$_N$2 oxidative addition (**TS2**) is preceded by a geometry distortion of **2** to adopt a tetrahedral geometry in **2′**, in which the spin is predominantly located on nickel. This more nucleophilic nickel center **2′**, although it proceeds to a nearly barrierless S$_N$2 attack on BnBr, is less stable than **2** by 10.4 kcal/mol,[64] resulting in an overall higher barrier relative to that of halogen-atom abstraction. Finally, the activation free energy of the outer-sphere concerted dissociative electron transfer (DET) mechanism was calculated using the modified Marcus theory (*i.e.*, the sticky model)[63,65,66] and gave a higher activation barrier ($\Delta G^{\ddagger} = 15.6$ kcal/mol) than halogen-atom abstraction.

We then studied the electronic effects of the nickelate [(bpy)Ni(aryl)Br]$^{\bullet-}$ complex by varying the *para*-substituents on the aryl group. [(bpy)Ni(aryl)Br]$^{\bullet-}$ complexes, bearing *p*-methoxy, -methyl, and -cyano substituents, all show similar activation energies toward BnBr (Figure 9). The similar reactivities of these nickel complexes agree with the experimental observations (Figure 6). We attribute this negligible electronic effect to the redox activity of bpy in **TS1**. When BnBr approaches the square-planar nickel center from the apical position, the unpaired electron is mainly delocalized to the bpy ligand. This electronic structure dilutes the electronic effect of *para*-substituents of the aryl group on the Ni center and, thus, results in insignificant changes of the rate.

The steric effects of the nickelate complexes bearing different aryl groups and the electronic effects of the alkyl halide electrophiles were also investigated computationally (*cf.* Tables S9 and S10, SI). The computed activation barriers are sensitive to these effects—halogen-atom transfer is faster with less hindered aryl ligands and with electron-deficient benzyl bromides. These trends are in qualitative agreement with the experimental observations (Figures 4 and 5).

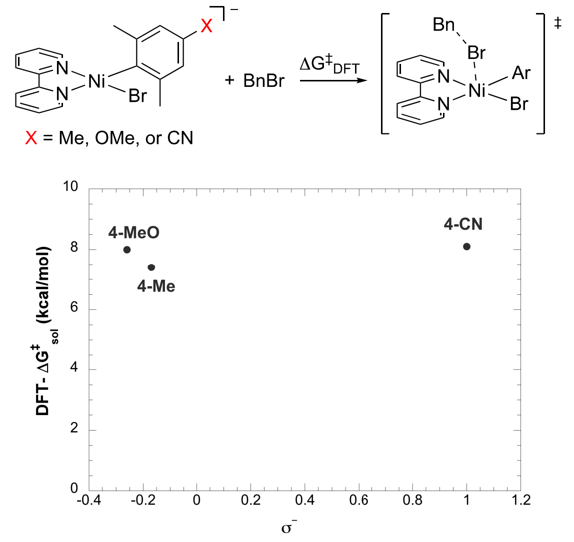

Figure 9. Computed activation free energies with *para*-substituted aryl nickelate complexes.

■ DISCUSSION

Concerted Halogen-Atom Dissociation Pathway. Comparing the reactivity of various electrophiles reveals that **2** is inactive toward C(sp^2) electrophiles (Figure 2A). This observation is reminiscent of a previous mechanistic study, where the activation of C(sp^2) electrophiles is conducted by Ni(I)−halides rather than Ni(I)−aryl species.[13] Among alkyl bromide electrophiles, the primary 1-bromopropane reacts slower than *t*BuBr and benzyl bromides. This trend disagrees with the oxidative addition mechanism, which would favor primary alkyl bromides (Scheme 3). DFT calculations reveal that the S$_N$2 pathway requires the distortion of square planar **2** to tetrahedral **2′**, and this endergonic process is less favorable than halogen-atom abstraction (Figure 8). The increase of the steric hindrance on Ni(I) decreases the rate of electrophile activation (Figure 4). This observation rules out the outer-sphere electron transfer (OSET) mechanism, since OSET would be insensitive to the steric effect of the nickel center.[67]

Scheme 3. Summary of Data that Supports the Concerted Halogen-Atom Dissociation Mechanism

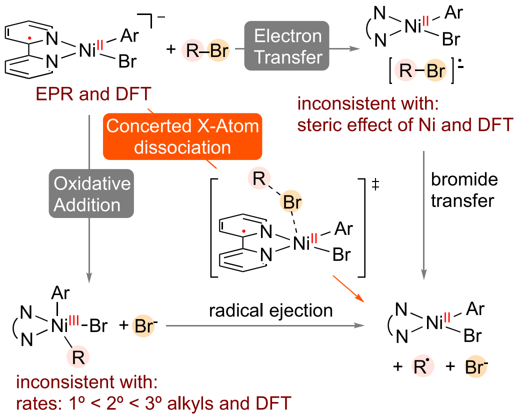

This assignment is consistent with DFT and Marcus theory calculations.

Experimental and computational data are consistent with a concerted halogen-atom dissociation pathway (Scheme 3, orange pathway). The Hammett study of the electronic effect of benzyl bromides has shed light on the nature of the transition state (Figure 5). Multiparameter linear regression analysis suggests the formation of both radical and partial negative charges at the benzylic carbon of the electrophile, evident by the positive coefficients of both $\sigma^{\bullet}_{\mathrm{JJ}}$ and σ^- terms. The polar term σ^- reflects the nucleophilic attack of the electron-rich nickel(I) center to the σ^* orbital of benzyl bromide that creates a partial negative charge. The radical term $\sigma^{\bullet}_{\mathrm{JJ}}$ suggests homolytic C−Br bond cleavage that gives rise to the radical character on the benzyl carbon. This description is corroborated by the DFT calculations. In the halogen-atom abstraction transition state, **TS1**, significant negative charge (−0.363) on the benzylic carbon of BnBr reveals a strong electron-transfer character in the process, whereas the spin density of 0.179 illustrates partial bond homolysis. After **TS1**, the halide never transferred to the metal center but spontaneously dissociated. Although having an analogous transition state, this process differs from a typical inner-sphere halogen-atom abstraction, which involves halide transfer to the metal center.[62,63] Thus, this mechanism is best described as an inner-sphere electron transfer (ISET) occurring concertedly with the dissociation of the halogen atom.

The kinetics of the reaction complies with that of halogen-atom abstraction, since these transition states both engage relatively strong interactions between nickel and the halogen atom and involve carbon−halogen bond dissociation. A linear free-energy relationship between the activation energy $\Delta G^\ddagger$ and the BDFE of the carbon−halogen bond of the electrophile, spanning chlorides, bromides, and iodides, demonstrates a preference for substrates that contain weak carbon−halogen bonds (Figure 2B). The slope of 0.24 in the linear fitting is within the range of slopes reported for halogen-atom abstraction by silyl, germanyl, and stannyl radicals (0.13−0.35).[68,69] The kinetics of halogen-atom abstraction promoted by sodium metal was historically modeled by the crossing of the Morse curves for the reactants and products to give a linear correlation of the activation energy ($\Delta G^\ddagger$) to the bond dissociation energy (ΔH) (eq 5).[70−72] The slope, ρ, depicts the shapes of the pretransition and post-transition state sections of the potential-energy curve. Savéant modified the Marcus theory by replacing the inner-sphere reorganization energy with the $\mathrm{BDFE}_{(\mathrm{C-X})}$ of the carbon−halogen bond to describe concerted halogen-atom dissociation upon outer-sphere electroreduction.[65,73] Through a range of electrophiles, this model predicts a linear correlation between $\Delta G^{\ddagger\ddagger}$ and $\mathrm{BDFE}_{(\mathrm{C-X})}$ with a slope approximated to 0.25. Studies are underway to build a model for describing inner-sphere halogen-atom abstraction/dissociation.

$$\Delta G^\ddagger = \rho \Delta H \tag{5}$$

Scheme 4. Preference of Ni(I) Species Reacting with $C(sp^2)$ and $C(sp^3)$ Electrophiles

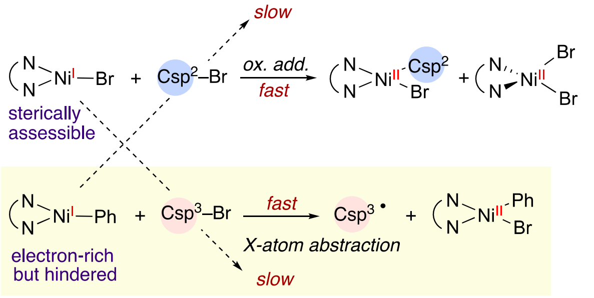

Implications for Cross-Electrophile Coupling. Elucidating the mechanism of Ni(I)-mediated halogen-atom abstraction has several implications for nickel-catalyzed cross-electrophile coupling reactions. In an earlier mechanistic investigation, we discovered that $C(sp^2)$ and $C(sp^3)$ electrophiles are sequentially activated through different pathways to generate Ni−aryl intermediates and alkyl radicals, respectively (Scheme 4).[13] The sequential reduction mechanism accounts for the selectivity of cross-electrophile coupling over homocoupling. This study provides further support to this hypothesis. $[(\mathrm{bpy})\mathrm{Ni}(\mathrm{Mes})\mathrm{Br}]^{\bullet-}$ (**2**) proved to mediate a faster activation of $C(sp^3)$ relative to $C(sp^2)$ electrophiles. The slower rate of $[(\mathrm{bpy})\mathrm{Ni}(\mathrm{Mes})\mathrm{Br}]^{\bullet-}$ (**2**) with $C(sp^2)$ electrophiles stems from the steric hindrance that prevents oxidative addition through a three-centered transition state. The coordination of the aryl group on nickel, as a strong σ-donor ligand, gives a more electron-rich **2** relative to (bpy)NiBr, which facilitates the activation of $C(sp^3)$ electrophiles to form radicals. The reactivity of (bpy)Ni(I)Br is not discussed here, and an investigation into the mechanism of (bpy)Ni(I)Br-mediated electrophile activation is underway.

The activation of $C(sp^3)$ electrophiles via halogen-atom abstraction dictates that the reactivity of electrophiles in catalytic cross-coupling is dependent on the BDE of the corresponding carbon−halogen and nickel−halogen bonds. Traveling up the periodic table from iodides to fluorides, the BDEs of both carbon−halogen and nickel−halogen bonds increase. The correlation of $\mathrm{BDE}_{(\mathrm{Ni-X})}$[74] vs $\mathrm{BDE}_{(\mathrm{C-X})}$[75] fits a linear function with a slope ranging from 0.58 to 0.69 for a series of alkyl halides (Figure 10). The slope values are lower than 1, suggesting that the increase of $\mathrm{BDE}_{(\mathrm{Ni-X})}$ from iodides to fluorides is slower than the increase of $\mathrm{BDE}_{(\mathrm{C-X})}$. As a result, the driving force for Ni-mediated electrophile activation decreases in the series from iodides to fluorides, hence the decrease of the rates.

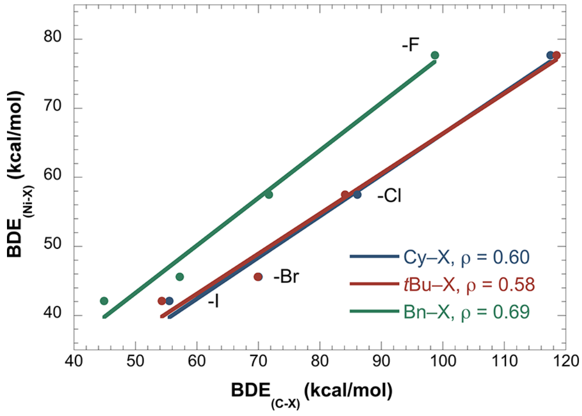

Figure 10. Correlation of $\mathrm{BDE}_{(\mathrm{Ni-X})}$ to $\mathrm{BDE}_{(\mathrm{C-X})}$.

Comparing alkyl halides as substrates in cross-coupling reactions, alkyl iodides are activated fastest but are often susceptible to homocoupling, owing to the direct reduction by zinc or manganese (Scheme 5).[76] The strong C−Cl bonds of

Scheme 5. Reactivity of $C(sp^3)$ Electrophiles

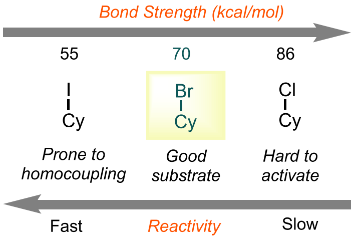

alkyl chlorides resist chlorine-atom abstraction by monovalent (bpy)Ni species; their activation requires alternative approaches. Cross-coupling of alkyl chlorides has been achieved by invoking halide exchange with bromides,[77] applying more-reducing Ni(0) species,[78,79] and promoting chlorine-atom abstraction by silyl radicals.[80] The bond strengths of alkyl bromides result in a suitable rate of bromine-atom abstraction by monovalent (bpy)Ni complexes that enables the radical to enter the catalytic cycle. Therefore, alkyl bromides serve as the most common electrophiles in these coupling reactions. Among alkyl bromides, the rate difference between primary, secondary, and tertiary substrates is rather small, whereas benzylic bromides react significantly faster.

The rate of halogen-atom abstraction is to some extent insensitive to the electronic effect of the aryl groups on nickel, providing a basis for accommodating a broad scope of $C(sp^2)$ electrophiles in coupling reactions. The electronic effect of the ligand appears to be insignificant on the activation of $C(sp^3)$ electrophiles, as evident by the similar rates between bpy and 4,4′-*t*Bu-bpy (Figure 6). The lack of an electronic effect is attributed to the redox activity of bpy and derivatives,[28,81] which dilutes the electronic effect of spectator ligands on the nickel center. The success of 4,4′-*t*Bu-bpy in nickel-catalyzed cross-coupling reactions may be attributed to its excellent solubility in organic solvents or an improved reactivity of other steps in the catalytic cycle.

■ SUMMARY

Electroanalytical studies reveal that monovalent (bpy)Ni complexes favor the activation of $C(sp^3)$ over $C(sp^2)$ electrophiles, which is ascribed to the cross-electrophile selectivity over homocoupling in cross-electrophile coupling reactions. The electronic and steric effects of nickel and the electrophile and the linear free-energy relationship between the activation free energy and the $BDFE_{(C-X)}$, in conjunction with DFT calculations, rule out the oxidative addition and outer-sphere electron transfer pathways and support an ISET/halogen-atom dissociation mechanism. The Hammett correlation of the electrophiles, corroborated with DFT findings, depicts a concerted early transition state that adopts substantial negative charge and radical character on the alkyl halide. The rate of nickel-mediated halogen-atom dissociation, dictated by the $BDE_{(C-X)}$, follows the model developed for halogen-atom abstraction, which accounts for the excellent reactivity of alkyl bromides in cross-coupling reactions. The rate of $C(sp^3)$ electrophile activation appears to be insensitive to the electronic effect of the spectator ligands, which is attributed to the redox activity of bpy.

■ ASSOCIATED CONTENT

Supporting Information

The Supporting Information is available free of charge at https://pubs.acs.org/doi/10.1021/jacs.1c05255.

All experimental procedures, additional figures, details of DFT calculations, CV measurements, and UV−vis and NMR spectra (PDF)

■ AUTHOR INFORMATION

Corresponding Authors

Peng Liu − *Department of Chemistry, University of Pittsburgh, Pittsburgh, Pennsylvania 15260, United States;* orcid.org/0000-0002-8188-632X; Email: pengliu@pitt.edu

Tianning Diao − *Department of Chemistry, New York University, New York, New York 10003, United States;* orcid.org/0000-0003-3916-8372; Email: diao@nyu.edu

Authors

Qiao Lin − *Department of Chemistry, New York University, New York, New York 10003, United States*

Yue Fu − *Department of Chemistry, University of Pittsburgh, Pittsburgh, Pennsylvania 15260, United States*

Complete contact information is available at: https://pubs.acs.org/10.1021/jacs.1c05255

Notes

The authors declare no competing financial interest.

■ ACKNOWLEDGMENTS

This work was supported by the National Institute of Health (R01 GM-127778) and the National Science Foundation (CHE-1654122). T.D. thanks the Alfred P. Sloan Foundation (FG-2018-10354) and the Camille and Henry Dreyfus Foundation (TC-19-019) for providing fellowships to partially support this work. T.D. acknowledges NSF (1827902) for funding to acquire the EPR spectrometer. P.L. thanks Pitt CRC, XSEDE, and TACC Frontera for supercomputer resources.

■ REFERENCES

(1) Tasker, S. Z.; Standley, E. A.; Jamison, T. F. Recent advances in homogeneous nickel catalysis. *Nature* **2014**, *509*, 299−309.

(2) Choi, J.; Fu, G. C. Transition metal−catalyzed alkyl-alkyl bond formation: Another dimension in cross-coupling chemistry. *Science* **2017**, *356*, eaaf7230.

(3) Fu, G. C. Transition-Metal Catalysis of Nucleophilic Substitution Reactions: A Radical Alternative to S_N1 and S_N2 Processes. *ACS Cent. Sci.* **2017**, *3*, 692−700.

(4) Diccianni, J. B.; Diao, T. Mechanisms of Nickel-Catalyzed Cross-Coupling Reactions. *Trends in Chemistry* **2019**, *1*, 830−844.

(5) Jones, G. D.; Martin, J. L.; McFarland, C.; Allen, O. R.; Hall, R. E.; Haley, A. D.; Brandon, R. J.; Konovalova, T.; Desrochers, P. J.; Pulay, P.; Vicic, D. A. Ligand Redox Effects in the Synthesis, Electronic Structure, and Reactivity of an Alkyl−Alkyl Cross-Coupling Catalyst. *J. Am. Chem. Soc.* **2006**, *128*, 13175−13183.

(6) Breitenfeld, J.; Ruiz, J.; Wodrich, M. D.; Hu, X. Bimetallic Oxidative Addition Involving Radical Intermediates in Nickel-Catalyzed Alkyl−Alkyl Kumada Coupling Reactions. *J. Am. Chem. Soc.* **2013**, *135*, 12004−12012.

(7) Biswas, S.; Weix, D. J. Mechanism and Selectivity in Nickel-Catalyzed Cross-Electrophile Coupling of Aryl Halides with Alkyl Halides. *J. Am. Chem. Soc.* **2013**, *135*, 16192−16197.

(8) Schley, N. D.; Fu, G. C. Nickel-Catalyzed Negishi Arylations of Propargylic Bromides: A Mechanistic Investigation. *J. Am. Chem. Soc.* **2014**, *136*, 16588−16593.

(9) Kc, S.; Dhungana, R. K.; Shrestha, B.; Thapa, S.; Khanal, N.; Basnet, P.; Lebrun, R. W.; Giri, R. Ni-Catalyzed Regioselective Alkylarylation of Vinylarenes via C(sp3)−C(sp3)/C(sp3)−C(sp2) Bond Formation and Mechanistic Studies. *J. Am. Chem. Soc.* **2018**, *140*, 9801−9805.

(10) Wang, X.; Ma, G.; Peng, Y.; Pitsch, C. E.; Moll, B. J.; Ly, T. D.; Wang, X.; Gong, H. Ni-Catalyzed Reductive Coupling of Electron-Rich Aryl Iodides with Tertiary Alkyl Halides. *J. Am. Chem. Soc.* **2018**, *140*, 14490−14497.

(11) Shu, W.; Garcia-Dominguez, A.; Quiros, M. T.; Mondal, R.; Cardenas, D. J.; Nevado, C. Ni-Catalyzed Reductive Dicarbofunctionalization of Nonactivated Alkenes: Scope and Mechanistic Insights. *J. Am. Chem. Soc.* **2019**, *141*, 13812−13821.

(12) Yin, H.; Fu, G. C. Mechanistic Investigation of Enantioconvergent Kumada Reactions of Racemic α-Bromoketones Catalyzed by a Nickel/Bis(oxazoline) Complex. *J. Am. Chem. Soc.* **2019**, *141*, 15433−15440.

(13) Lin, Q.; Diao, T. Mechanism of Ni-Catalyzed Reductive 1,2-Dicarbofunctionalization of Alkenes. *J. Am. Chem. Soc.* **2019**, *141*, 17937−17948.

(14) Cherney, A. H.; Kadunce, N. T.; Reisman, S. E. Enantioselective and Enantiospecific Transition-Metal-Catalyzed Cross-Coupling Reactions of Organometallic Reagents to Construct C−C Bonds. *Chem. Rev.* **2015**, *115*, 9587−9652.

(15) Lucas, E. L.; Jarvo, E. R. Stereospecific and Stereoconvergent Cross-Couplings Between Alkyl Electrophiles. *Nat. Rev. Chem.* **2017**, *1*, 0065.

(16) Funes-Ardoiz, I.; Nelson, D. J.; Maseras, F. Halide Abstraction Competes with Oxidative Addition in the Reactions of Aryl Halides with $[\mathrm{Ni(PMe_nPh_{(3-n))4}}]$. *Chem. - Eur. J.* **2017**, *23*, 16728−16733.

(17) Bakac, A.; Espenson, J. H. Kinetics and mechanism of the alkylnickel formation in one-electron reductions of alkyl halides and hydroperoxides by a macrocyclic nickel(I) complex. *J. Am. Chem. Soc.* **1986**, *108*, 713−719.

(18) Ozaki, S.; Matsushita, H.; Ohmori, H. Indirect electroreductive cyclisation of N-allylic and N-propargylbromo amides and o-bromoacryloylanilides using nickel(II) complexes as electron-transfer catalysts. *J. Chem. Soc., Perkin Trans. 1* **1993**, *19*, 2339−2344.

(19) Duñach, E.; José Medeiros, M.; Olivero, S. Intramolecular reductive cyclisations using electrochemistry: development of environmentally friendly synthetic methodologies. *New J. Chem.* **2006**, *30*, 1534−1548.

(20) Foley, M. P.; Du, P.; Griffith, K. J.; Karty, J. A.; Mubarak, M. S.; Raghavachari, K.; Peters, D. G. Electrochemistry of substituted salen complexes of nickel(II): Nickel(I)-catalyzed reduction of alkyl and acetylenic halides. *J. Electroanal. Chem.* **2010**, *647*, 194−203.

(21) Martin, E. T.; McGuire, C. M.; Peters, D. G. Catalytic Reduction of Organic Halides by Electrogenerated Nickel(I) Salen. *Electrochem. Soc. Interface* **2016**, *25*, 41−45.

(22) Duñach, E.; Medeiros, M. J.; Olivero, S. Electrochemical cyclizations of organic halides catalyzed by electrogenerated nickel(I) complexes: towards environmentally friendly methodologies. *Electrochim. Acta* **2017**, *242*, 373−381.

(23) Lin, X.; Phillips, D. L. Density Functional Theory Studies of Negishi Alkyl−Alkyl Cross-Coupling Reactions Catalyzed by a Methylterpyridyl-Ni(I) Complex. *J. Org. Chem.* **2008**, *73*, 3680−3688.

(24) Yoo, C.; Ajitha, M. J.; Jung, Y.; Lee, Y. Mechanistic Study on C−C Bond Formation of a Nickel(I) Monocarbonyl Species with Alkyl Iodides: Experimental and Computational Investigations. *Organometallics* **2015**, *34*, 4305−4311.

(25) Lin, X.; Sun, J.; Xi, Y.; Lin, D. How Racemic Secondary Alkyl Electrophiles Proceed to Enantioselective Products in Negishi Cross-Coupling Reactions. *Organometallics* **2011**, *30*, 3284−3292.

(26) Laskowski, C. A.; Bungum, D. J.; Baldwin, S. M.; Del Ciello, S. A.; Iluc, V. M.; Hillhouse, G. L. Synthesis and Reactivity of Two-Coordinate Ni(I) Alkyl and Aryl Complexes. *J. Am. Chem. Soc.* **2013**, *135*, 18272−18275.

(27) Diccianni, J. B.; Katigbak, J.; Hu, C.; Diao, T. Mechanistic Characterization of (Xantphos)Ni(I)-Mediated Alkyl Bromide Activation: Oxidative Addition, Electron Transfer, or Halogen-Atom Abstraction. *J. Am. Chem. Soc.* **2019**, *141*, 1788−1796.

(28) Mohadjer Beromi, M.; Brudvig, G. W.; Hazari, N.; Lant, H. M. C.; Mercado, B. Q. Synthesis and Reactivity of Paramagnetic Nickel Polypyridyl Complexes Relevant to $\mathrm{C(sp^2)-C(sp^3)}$ Coupling Reactions. *Angew. Chem., Int. Ed.* **2019**, *58*, 6094−6098.

(29) Rountree, E. S.; McCarthy, B. D.; Eisenhart, T. T.; Dempsey, J. L. Evaluation of Homogeneous Electrocatalysts by Cyclic Voltammetry. *Inorg. Chem.* **2014**, *53*, 9983−10002.

(30) Lee, K. J.; Elgrishi, N.; Kandemir, B.; Dempsey, J. L. Electrochemical and spectroscopic methods for evaluating molecular electrocatalysts. *Nat. Rev. Chem.* **2017**, *1*, 0039.

(31) Sandford, C.; Edwards, M. A.; Klunder, K. J.; Hickey, D. P.; Li, M.; Barman, K.; Sigman, M. S.; White, H. S.; Minteer, S. D. A synthetic chemist's guide to electroanalytical tools for studying reaction mechanisms. *Chem. Sci.* **2019**, *10*, 6404−6422.

(32) Labbé, E.; Buriez, O. Fundamental Input of Analytical Electrochemistry in the Determination of Intermediates and Reaction Mechanisms in Electrosynthetic Processes. *ChemElectroChem* **2019**, *6*, 4118−4125.

(33) Sandford, C.; Fries, L. R.; Ball, T. E.; Minteer, S. D.; Sigman, M. S. Mechanistic Studies into the Oxidative Addition of Co(I) Complexes: Combining Electroanalytical Techniques with Parameterization. *J. Am. Chem. Soc.* **2019**, *141*, 18877−18889.

(34) Tang, T.; Sandford, C.; Minteer, S. D.; Sigman, M. S. Analyzing mechanisms in Co(I) redox catalysis using a pattern recognition platform. *Chem. Sci.* **2021**, *12*, 4771−4778.

(35) Wuttig, A.; Derrick, J. S.; Loipersberger, M.; Snider, A.; Head-Gordon, M.; Chang, C. J.; Toste, F. D. Controlled Single-Electron Transfer via Metal−Ligand Cooperativity Drives Divergent Nickel-Electrocatalyzed Radical Pathways. *J. Am. Chem. Soc.* **2021**, *143*, 6990−7001.

(36) Amatore, C.; Jutand, A. Rates and mechanism of biphenyl synthesis catalyzed by electrogenerated coordinatively unsaturated nickel complexes. *Organometallics* **1988**, *7*, 2203−2214.

(37) Durandetti, M.; Nédélec, J.-Y.; Périchon, J. Nickel-Catalyzed Direct Electrochemical Cross-Coupling between Aryl Halides and Activated Alkyl Halides. *J. Org. Chem.* **1996**, *61*, 1748−1755.

(38) Yakhvarov, D. G.; Budnikova, Y. H.; Sinyashin, O. G. Kinetic features of oxidative addition of organic halides to the organonickel σ-complex. *Russ. Chem. Bull.* **2003**, *52*, 567−569.

(39) Kawamata, Y.; Vantourout, J. C.; Hickey, D. P.; Bai, P.; Chen, L.; Hou, Q.; Qiao, W.; Barman, K.; Edwards, M. A.; Garrido-Castro, A. F.; deGruyter, J. N.; Nakamura, H.; Knouse, K.; Qin, C.; Clay, K. J.; Bao, D.; Li, C.; Starr, J. T.; Garcia-Irizarry, C.; Sach, N.; White, H. S.; Neurock, M.; Minteer, S. D.; Baran, P. S. Electrochemically Driven, Ni-Catalyzed Aryl Amination: Scope, Mechanism, and Applications. *J. Am. Chem. Soc.* **2019**, *141*, 6392−6402.

(40) Klein, A.; Kaiser, A.; Sarkar, B.; Wanner, M.; Fiedler, J. The electrochemical behaviour of organonickel complexes: Mono-, di- and trivalent nickel. *Eur. J. Inorg. Chem.* **2007**, *2007*, 965−976.

(41) Klein, A.; Kaiser, A.; Wielandt, W.; Belaj, F.; Wendel, E.; Bertagnolli, H.; Záliš, S. Halide Ligands—More Than Just σ-Donors? A Structural and Spectroscopic Study of Homologous Organonickel Complexes. *Inorg. Chem.* **2008**, *47*, 11324−11333.

(42) Francke, R.; Little, R. D. Redox catalysis in organic electrosynthesis: basic principles and recent developments. *Chem. Soc. Rev.* **2014**, *43*, 2492−2521.

(43) Yan, M.; Kawamata, Y.; Baran, P. S. Synthetic Organic Electrochemical Methods Since 2000: On the Verge of a Renaissance. *Chem. Rev.* **2017**, *117*, 13230−13319.

(44) Kingston, C.; Palkowitz, M. D.; Takahira, Y.; Vantourout, J. C.; Peters, B. K.; Kawamata, Y.; Baran, P. S. A Survival Guide for the "Electro-curious". *Acc. Chem. Res.* **2020**, *53*, 72−83.

(45) Everson, D. A.; Shrestha, R.; Weix, D. J. Nickel-Catalyzed Reductive Cross-Coupling of Aryl Halides with Alkyl Halides. *J. Am. Chem. Soc.* **2010**, *132*, 920−921.

(46) Nicholson, R. S.; Shain, I. Theory of Stationary Electrode Polarography. Single Scan and Cyclic Methods Applied to Reversible, Irreversible, and Kinetic Systems. *Anal. Chem.* **1964**, *36*, 706−723.

(47) Cannes, C.; Labbé, E.; Durandetti, M.; Devaud, M.; Nédélec, J. Y. Nickel-catalyzed electrochemical homocoupling of alkenyl halides: rates and mechanisms. *J. Electroanal. Chem.* **1996**, *412*, 85−93.

(48) BDFE values in Figure 2 were taken from the following reference: Lin, C. Y.; Peh, J.; Coote, M. L. Effects of Chemical Structure on the Thermodynamic Efficiency of Radical Chain Carriers for Organic Synthesis. *J. Org. Chem.* **2011**, *76*, 1715−1726.

(49) Lee, C.; Xu, L.; Singhal, M.; Mendes, P.; Hoops, S.; Pahle, J.; Simus, N.; Gauges, R.; Sahle, S.; Kummer, U. COPASI—a COmplex PAthway SImulator. *Bioinformatics* **2006**, *22*, 3067−3074.

(50) Costentin, C.; Savéant, J.-M. Multielectron, Multistep Molecular Catalysis of Electrochemical Reactions: Benchmarking of Homogeneous Catalysts. *ChemElectroChem* **2014**, *1*, 1226−1236.

(51) Costentin, C.; Drouet, S.; Robert, M.; Savéant, J.-M. Turnover Numbers, Turnover Frequencies, and Overpotential in Molecular Catalysis of Electrochemical Reactions. Cyclic Voltammetry and Preparative-Scale Electrolysis. *J. Am. Chem. Soc.* **2012**, *134*, 11235−11242.

(52) Wasylenko, D. J.; Rodríguez, C.; Pegis, M. L.; Mayer, J. M. Direct Comparison of Electrochemical and Spectrochemical Kinetics for Catalytic Oxygen Reduction. *J. Am. Chem. Soc.* **2014**, *136*, 12544−12547.

(53) Wang, V. C. C.; Johnson, B. A. Interpreting the Electrocatalytic Voltammetry of Homogeneous Catalysts by the Foot of the Wave Analysis and Its Wider Implications. *ACS Catal.* **2019**, *9*, 7109−7123.

(54) Jiang, X.-K.; Ding, W. F.-X.; Zhang, Y.-H. The nucleophilic silyl radical: Dual-parameter correlation analysis of the relative rates of bromine-atom abstraction reactions as measured by a rigorous methodology. *Tetrahedron* **1997**, *53*, 8479−8490.

(55) Kira, M.; Ishima, T.; Iwamoto, T.; Ichinohe, M. A Mechanistic Study of Reactions of Stable Disilenes with Haloalkanes. *J. Am. Chem. Soc.* **2001**, *123*, 1676−1682.

(56) Menapace, L. W.; Loewenthal, M. B.; Koscielecki, J.; Tucker, L.; Passaro, L. C.; Montalbano, R.; Frank, A. J.; Marrantino, J.; Brunner, J. Organotin Hydride Reduction of Benzyl Bromides. *Organometallics* **2002**, *21*, 3066−3068.

(57) Sigman, M. S.; Harper, K. C.; Bess, E. N.; Milo, A. The Development of Multidimensional Analysis Tools for Asymmetric Catalysis and Beyond. *Acc. Chem. Res.* **2016**, *49*, 1292−1301.

(58) Jiang, X.; Ji, G. A self-consistent and cross-checked scale of spin-delocalization substituent constants, the $\sigma^{\bullet}_{JJ}$ scale. *J. Org. Chem.* **1992**, *57*, 6051−6056.

(59) Jiang, X.-K. Establishment and Successful Application of the $\sigma^{\bullet}_{JJ}$ Scale of Spin-Delocalization Substituent Constants. *Acc. Chem. Res.* **1997**, *30*, 283−289.

(60) Yakhvarov, D. G.; Petr, A.; Kataev, V.; Büchner, B.; Gómez-Ruiz, S.; Hey-Hawkins, E.; Kvashennikova, S. V.; Ganushevich, Y. S.; Morozov, V. I.; Sinyashin, O. G. Synthesis, structure and electrochemical properties of the organonickel complex [NiBr(Mes)(phen)] (Mes = 2,4,6-trimethylphenyl, phen = 1,10-phenanthroline). *J. Organomet. Chem.* **2014**, *750*, 59−64.

(61) Ma, Q.; Werner, H.-J. Scalable Electron Correlation Methods. 8. Explicitly Correlated Open-Shell Coupled-Cluster with Pair Natural Orbitals PNO-RCCSD(T)-F12 and PNO-UCCSD(T)-F12. *J. Chem. Theory Comput.* **2021**, *17*, 902−926.

(62) Lin, C. Y.; Coote, M. L.; Gennaro, A.; Matyjaszewski, K. Ab Initio Evaluation of the Thermodynamic and Electrochemical Properties of Alkyl Halides and Radicals and Their Mechanistic Implications for Atom Transfer Radical Polymerization. *J. Am. Chem. Soc.* **2008**, *130*, 12762−12774.

(63) Fang, C.; Fantin, M.; Pan, X.; de Fiebre, K.; Coote, M. L.; Matyjaszewski, K.; Liu, P. Mechanistically Guided Predictive Models for Ligand and Initiator Effects in Copper-Catalyzed Atom Transfer Radical Polymerization (Cu-ATRP). *J. Am. Chem. Soc.* **2019**, *141*, 7486−7497.

(64) Ting, S. I.; Garakyaraghi, S.; Taliaferro, C. M.; Shields, B. J.; Scholes, G. D.; Castellano, F. N.; Doyle, A. G. 3d-d Excited States of Ni(II) Complexes Relevant to Photoredox Catalysis: Spectroscopic Identification and Mechanistic Implications. *J. Am. Chem. Soc.* **2020**, *142*, 5800−5810.

(65) Saveant, J. M. Dissociative electron transfer. New tests of the theory in the electrochemical and homogeneous reduction of alkyl halides. *J. Am. Chem. Soc.* **1992**, *114*, 10595−10602.

(66) The stepwise outer-sphere single-electron transfer/radical anion dissociation pathway was not considered computationally, because we cannot locate the radical anion ($BnBr^{\bullet-}$) in our calculations—the bromide anion spontaneously dissociates from the radical anion in geometry optimization, indicating that the $BnBr^{\bullet-}$ radical anion is not stable. Therefore, we only considered a concerted outer-sphere dissociative single-electron transfer that directly leads to the benzyl radical and bromide anion.

(67) Wong, C. L.; Kochi, J. K. Electron Transfer with Organometals. Steric Effects as Probes for Outer-Sphere and Inner-Sphere Oxidations of Homoleptic Alkylmetals with Iron(III) and Iridate(IV) Complexes. *J. Am. Chem. Soc.* **1979**, *101*, 5593−5603.

(68) Ingold, K. U.; Lusztyk, J.; Scaiano, J. C. Absolute rate constants for the reactions of tributylgermyl and tributylstannyl radicals with carbonyl compounds, other unsaturated molecules, and organic halides. *J. Am. Chem. Soc.* **1984**, *106*, 343−348.

(69) Ito, O.; Hoteiya, K.; Watanabe, A.; Matsuda, M. Flash Photolysis Study for Halogen Abstraction of and $Ph_3Sn\cdot$ and $Ph_3Si\cdot$ from Alkyl Halides. *Bull. Chem. Soc. Jpn.* **1991**, *64*, 962−965.

(70) Evans, M. G.; Warhurst, E. The mechanism of reactions between alkali metal atoms and methyl and phenyl halides. *Trans. Faraday Soc.* **1939**, *35*, 593−606.

(71) Butler, E. T.; Polanyi, M. Rates of pyrolysis and bond energies of substituted organic iodides (Part I). *Trans. Faraday Soc.* **1943**, *39*, 19−36.

(72) Warhurst, E. The sodium "flame" reactions. *Q. Rev., Chem. Soc.* **1951**, *5*, 44−59.

(73) Costentin, C.; Louault, C.; Robert, M.; Roge, V.; Saveant, J. M. Reorganization energy and pre-exponential factor from temperature-dependent experiments in electron transfer reactions. A typical example: the reduction of tert-nitrobutane. *Phys. Chem. Chem. Phys.* **2012**, *14*, 1581−1584.

(74) $BDE_{(Ni-X)}$ values were calculated for the Ni−X bond in $[(bpy)Ni(Mes)BrX]^-$, a complex that resembles the transition state.

(75) Luo, Y.-R. *Comprehensive Handbook of Chemical Bond Energies*; CRC Press: Boca Raton, FL, 2007.

(76) Wright, T. H.; Bower, B. J.; Chalker, J. M.; Bernardes, G. J. L.; Wiewiora, R.; Ng, W.-L.; Raj, R.; Faulkner, S.; Vallée, M. R. J.; Phanumartwiwath, A.; Coleman, O. D.; Thézénas, M.-L.; Khan, M.; Galan, S. R. G.; Lercher, L.; Schombs, M. W.; Gerstberger, S.; Palm-Espling, M. E.; Baldwin, A. J.; Kessler, B. M.; Claridge, T. D. W.; Mohammed, S.; Davis, B. G. Posttranslational mutagenesis: A chemical strategy for exploring protein side-chain diversity. *Science* **2016**, *354*, aag1465.

(77) Kim, S.; Goldfogel, M. J.; Gilbert, M. M.; Weix, D. J. Nickel-Catalyzed Cross-Electrophile Coupling of Aryl Chlorides with Primary Alkyl Chlorides. *J. Am. Chem. Soc.* **2020**, *142*, 9902−9907.

(78) Lu, Z.; Fu, G. C. Alkyl−Alkyl Suzuki Cross-Coupling of Unactivated Secondary Alkyl Chlorides. *Angew. Chem., Int. Ed.* **2010**, *49*, 6676−6678.

(79) Börjesson, M.; Moragas, T.; Martin, R. Ni-Catalyzed Carboxylation of Unactivated Alkyl Chlorides with CO_2. *J. Am. Chem. Soc.* **2016**, *138*, 7504−7507.

(80) Sakai, H. A.; Liu, W.; Le, C. C.; MacMillan, D. W. C. Cross-Electrophile Coupling of Unactivated Alkyl Chlorides. *J. Am. Chem. Soc.* **2020**, *142*, 11691−11697.

(81) Wagner, C. L.; Herrera, G.; Lin, Q.; Hu, C. T.; Diao, T. Redox Activity of Pyridine-Oxazoline Ligands in the Stabilization of Low-

Valent Organonickel Radical Complexes. *J. Am. Chem. Soc.* **2021**, *143*, 5295−5300.

https://doi.org/10.1021/jacs.1c05255